Chemical Science

ROYAL SOCIETY OF CHEMISTRY

EDGE ARTICLE

View Article Online
View Journal | View Issue

Cite this: *Chem. Sci.*, 2021, **12**, 13897

All publication charges for this article have been paid for by the Royal Society of Chemistry

Received 6th September 2021
Accepted 22nd September 2021

DOI: 10.1039/d1sc04913e

rsc.li/chemical-science

$Ba_4Ca(B_2O_5)_2F_2$: π-conjugation of B_2O_5 in the planar pentagonal layer achieving large second harmonic generation of *pyro*-borate†

Shuaishuai Li,‡[a] Xiaomeng Liu,‡[b] Hongping Wu,[a] Zhongfu Song,[a] Hongwei Yu,*[a] Zheshuai Lin,*[b] Zhanggui Hu,[a] Jiyang Wang[a] and Yicheng Wu[a]

The nonlinear optical (NLO) crystals that can expand the wavelength of the laser to the deep-ultraviolet (DUV) region by the cascaded second harmonic generation (SHG) are of current research interest. It is well known that borates are the most ideal material class for the design of new DUV NLO crystals owing to the presence of good NLO genes, *e.g.*, BO_3 or B_3O_6 groups. However, the NLO *pyro*-borates with the B_2O_5 dimers as the sole basic building units are still rarely reported owing to their small SHG responses. In this communication, by constructing a planar pentagonal $[Ca(B_2O_5)]_\infty$ layer, the NLO *pyro*-borate $Ba_4Ca(B_2O_5)_2F_2$ with a large SHG response (~2.2 × KDP, or ~7 × α-$Li_4B_2O_5$) and a DUV transparent window has been designed and synthesized. The first-principles calculations show that the large SHG response of $Ba_4Ca(B_2O_5)_2F_2$ mainly originates from the better π-conjugation of the coplanar B_2O_5 dimers in the $[Ca(B_2O_5)]_\infty$ layer. In addition, the planar pentagonal pattern in the $[Ca(B_2O_5)]_\infty$ layer provides an ideal template for designing the new DUV NLO crystals, apart from those in known DUV borates, *e.g.*, the $[Be_2BO_3F_2]_\infty$ layer in $KBe_2BO_3F_2$ (KBBF).

Deep-ultraviolet (DUV, $\lambda < 200$ nm) coherent lights with high photon energy, high spatial resolution, and a small heat-affected zone are of significance for applications in photolithography, high-resolution spectroscopy, laser cooling, and scientific equipment.[1–4] However, it is difficult or well-nigh impossible for solid-state lasers to directly radiate the DUV coherent lights. In contrast, relying on the process of second harmonic generation (SHG) of nonlinear optical (NLO) crystals is a more effective way to generate the DUV coherent lights and causes much attention.[5,6] Therefore, the NLO crystal has become an important material basis of solid-state lasers, which seriously affects the development of all-solid-state laser technology. However, it is still a great challenge to rationally design and synthesize DUV NLO crystals because of the extremely rigorous requirements of structural symmetry and properties.[7–10] Structurally, the DUV NLO crystals must crystallize in the noncentrosymmetric (NCS) space groups which are the prerequisite for the materials to exhibit SHG responses. Moreover, it should possess a broad transparency window, a largely effective NLO coefficient ($d_{eff} \geq 0.39$ pm V^{-1}), and a moderate birefringence (0.05–0.10@1064 nm) to achieve the phase-matching (PM) conditions in the DUV region.[10] Based on these requirements, borates have been considered as the ideal material class for DUV NLO crystals because of their special structure and properties' virtues, including the rich acentric structural types, large band gaps, and stable physical and chemical properties.[8] To date, the commercialized borate-based UV NLO crystals consist of β-BaB_2O_4 (BBO), LiB_3O_5 (LBO), $CsLiB_6O_{10}$ (CLBO),[9,10] and the practical DUV NLO crystal $KBe_2BO_3F_2$ (KBBF). Especially for KBBF, it has become the sole material that can generate DUV coherent laser light (177.3 nm) by a direct SHG method.[7] Other excellent borate-based UV NLO crystals also consist of $K_3B_6O_{10}Cl$,[11] $SrB_5O_7F_3$,[12] $Li_2B_6O_9F_2$,[5] $CsAlB_3O_6F$,[13] $M_2B_{10}O_{14}F_6$ (M = Ca, Sr),[14] $NH_4B_4O_6F$,[15] $NaSr_3Be_3B_3O_9F_4$,[16] AB_4O_6F (A = K, Rb, and Cs),[17] *etc.*

The above borate-based materials have achieved great success as UV and DUV NLO crystals, which are mainly attributed to the ability of boron atoms to coordinate with three or four oxygen anions forming trigonal-planar or tetrahedral building blocks.[18,19] For example, the first borate-based NLO crystal, $KB_5O_8 \cdot 4H_2O$ (KB_5), has the basic building units (BBUs) of $[B_5O_{10}]$, while the BBUs of β-BBO, LBO, and KBBF are $[B_3O_6]$, $[B_3O_7]$, and isolated $[BO_3]$, respectively.[7,8] Remarkably, although various borate crystals with different types of borate groups have been explored during the past decades, the *pyro*-borate

[a]*Tianjin Key Laboratory of Functional Crystal Materials, Institute of Functional Crystal, Tianjin University of Technology, Tianjin 300384, China. E-mail: hwyu15@gmail.com*

[b]*Beijing Center for Crystal R&D, Key Lab of Functional Crystals and Laser Technology of Chinese Academy of Sciences, Technical Institute of Physics and Chemistry, Chinese Academy of Sciences, Beijing 100190, P. R. China. E-mail: zslin@mail.ipc.ac.cn*

† Electronic supplementary information (ESI) available. CCDC 2095000. For ESI and crystallographic data in CIF or other electronic format see DOI: 10.1039/d1sc04913e

‡ Shuaishuai Li and Xiaomeng Liu contributed equally.

NLO crystals with B_2O_5 groups as the sole BBUs are rarely reported owing to their weak SHG responses.[20–23] For example, the SHG response of the DUV transparent α-$Li_4B_2O_5$ (ref. 23) is only ~0.3 × KDP, which is far smaller than the expected value (0.39 pm V^{-1}, 1 × KDP).

Actually, the flexible B_2O_5 groups which are composed of two π-conjugated BO_3 units through corner-sharing may also be capable of generating excellent optical performance if they have benign arrangements. In recent research, Pan's group has indicated that the B_2O_5 dimers are perfect for the design of DUV birefringent crystals. By the synergistic combination, they have successfully designed a potential *pyro*-borate birefringent crystal, $Li_2Na_2B_2O_5$, with a short UV cut-off edge (181 nm) and large birefringence (0.095@532 nm).[21] And they have also grown $Ca(BO_2)_2$ crystals exhibiting a short UV cut-off edge and larger birefringence (169 nm; 0.2471@193 nm). Based on the analysis of the structure–property relationship of $Ca(BO_2)_2$, they stated that the polymerized planar B_nO_{2n+1} groups, *e.g.*, B_2O_5, could generate a larger anisotropy than isolated BO_3.[22] However, their opposite arrangements of B–O groups make them crystallize in the centrosymmetric (CS) space groups, which limit their further development as NLO compounds. Thus, it is clear that *pyro*-borates exhibiting a large birefringence and a short UV cut-off edge would also be promising DUV NLO crystals if their SHG responses can be enhanced.

Based on the above-mentioned ideas, a systematical investigation has been performed on DUV *pyro*borates. And finally, we successfully synthesized a new NCS *pyro*-borate, $Ba_4Ca(B_2O_5)_2F_2$, which can exhibit not only a large SHG response (~2.2 × KDP and ~7 × α-$Li_4B_2O_5$) but also a short UV cut-off edge (<190 nm). Analyzing its structure, one can find that its excellent NLO properties mainly originate from the unique planar pentagonal $[Ca(B_2O_5)]_\infty$ layer, where the B_2O_5 groups adopt the almost coplanar configurations that favor the structure to generate large SHG response and birefringence,[21] meanwhile the terminal O atoms of B_2O_5 groups are also linked by the Ca^{2+} cations, which eliminate the dangling bonds of B_2O_5 groups and further blue-shift the UV cut-off edge. More importantly, the adjacent $[Ca(B_2O_5)]_\infty$ layers in $Ba_4Ca(B_2O_5)_2F_2$ are linked by other B_2O_5 groups to form a 3D framework, which will be favorable for the material to avoid the layer habit that KBBF suffers from. In this sense, the planar pentagonal $[Ca(B_2O_5)]_\infty$ layer is similar to the $[Be_2BO_3F_2]_\infty$ layer in KBBF, and it can be seen as a new structure template for the design of new DUV NLO crystals, especially for the DUV *pyro*-borates. Herein, we will describe the synthesis, experimental and computational characterization as well as the functional properties of the new DUV NLO material, $Ba_4Ca(B_2O_5)_2F_2$.

A polycrystalline sample of $Ba_4Ca(B_2O_5)_2F_2$ was synthesized by the conventional solid-state reaction and the purity was confirmed by powder X-ray diffraction (XRD) (Fig. S1†). With the polycrystalline sample, the thermal behavior of $Ba_4Ca(B_2O_5)_2F_2$ was studied by the thermogravimetric (TG) and differential scanning calorimetry (DSC) measurements. The heating DSC curve shows a sharp endothermic peak at 815 °C with no obvious weight loss in the TG curve (Fig. S2†), suggesting that $Ba_4Ca(B_2O_5)_2F_2$ has good thermal stability. To further investigate the thermal behavior of $Ba_4Ca(B_2O_5)_2F_2$, the polycrystalline sample was calcined at 840 °C and the XRD analysis showed that the calcined sample was $Ba_4Ca(B_2O_5)_2F_2$, $Ba_2Ca(BO_3)_2$ (PDF #01-085-2268), $Ba_2CaB_6O_{12}$ (PDF #01-075-1401) and other unknown phases (Fig. S3†). These results illustrate that $Ba_4Ca(B_2O_5)_2F_2$ melts incongruently and the suitable flux is necessary for the crystal growth.

With the Na_2O–PbF_2–B_2O_3 as the flux, millimeter-sized block crystals of $Ba_4Ca(B_2O_5)_2F_2$ were grown for the single-crystal XRD structure determination. $Ba_4Ca(B_2O_5)_2F_2$ crystallizes in the NCS and polar space group, $P2_1$ (Table S1†). In the asymmetric unit, there are four unique Ba, one Ca, four B, ten O, and two F atom(s), which all fully occupy the 2*a* Wyckoff positions (Table S2†). All B atoms are coordinated to three oxygen atoms to form the BO_3 triangles with the B–O distances ranging from 1.312(17) to 1.460(16) Å and O–B–O angles varying from 108.0(13) to 130.2(15)°. The BO_3 triangles are further connected to form two types of B_2O_5 dimers, *i.e.* plane $B(1,3)_2O_5$ and twisted $B(2,4)_2O_5$, which are the BBUs of $Ba_4Ca(B_2O_5)_2F_2$. The Ca atoms are coordinated to six oxygen atoms to form CaO_6 octahedra with the Ca–O distances ranging from 2.285(9) to 2.325(13) Å. For the Ba^{2+} cations, they exhibit three different coordination environments, $Ba(1,2)O_6F_2$, $Ba(3)O_8F_2$, and $Ba(4)O_7F_2$ (Fig. S4†) with the Ba–O distances ranging from 2.585(9) to 3.250(11) Å and the Ba–F bond lengths ranging from 2.635(8) to 2.736(8) Å. Remarkably, for the F^- anions, each unique fluorine atom serves as a common vertex for four Ba atoms to form the FBa_4 polyhedra (Fig. S5a†), which could be treated as fluorine-centered secondary building units (SBUs). The Ba–F–Ba angles vary from 99.0 (2) to 120.2 (3)°. The bond valence sum (BVS) calculations show the values of 1.67–1.97, 2.45, 2.88–3.10, 1.78–2.13, and 0.95–1.09, for Ba^{2+}, Ca^{2+} B^{3+}, O^{2-}, and F^-, respectively (Table S2†). The BVSs of atoms are consistent with their expected oxidation states except the one from the Ca^{2+} cations. The larger BVSs of Ca^{2+} cations can be attributed to six shorter Ca–O bond lengths, which are also observed in other Ca^{2+}-containing borates, such as $YCa_3(VO)_3(BO_3)_4$ (2.44),[24] $Rb_2Ca_3B_{16}O_{28}$ (2.29), and $Cs_2Ca_3B_{16}O_{28}$ (2.30).[25]

The structure of $Ba_4Ca(B_2O_5)_2F_2$ is shown in Fig. 1. In the structure, the plane $B(1,3)_2O_5$ dimer is first connected with four CaO_6 octahedra, meanwhile, each CaO_6 octahedron is also linked by four $B(1,3)_2O_5$ dimers through sharing their four equatorial O atoms to form a unique planar pentagonal $[Ca(B_2O_5)]_\infty$ layer in the *b*–*c* plane (Fig. 1a, b). Then, these $[Ca(B_2O_5)]_\infty$ layers are further linked by the twisted $B(2,4)_2O_5$ dimers to construct a 3D framework with Ba^{2+} cations maintaining the charge balance (Fig. 1c). Remarkably, for the arrangements of the Ba^{2+} cations and the F^- anions, the fluorine-centered SBU FBa_4 polyhedra are linked to construct the 2D $[F_2Ba_4]$ infinite layer (Fig. S5b†) with the same orientation, which further fills the apertures in the $[Ca(B_2O_5)_2]$ framework (Fig. S5c†). The existence of fluorine-centered SBUs would certainly have a strong influence on the local coordinate environments, and finally on the whole structure.[26]

It is very interesting that $Ba_4Ca(B_2O_5)_2F_2$ contains a planar pentagonal $[Ca(B_2O_5)]_\infty$ layer, which is similar to the $[Be_2BO_3F_2]_\infty$ layer in KBBF. The structural evolution from KBBF to

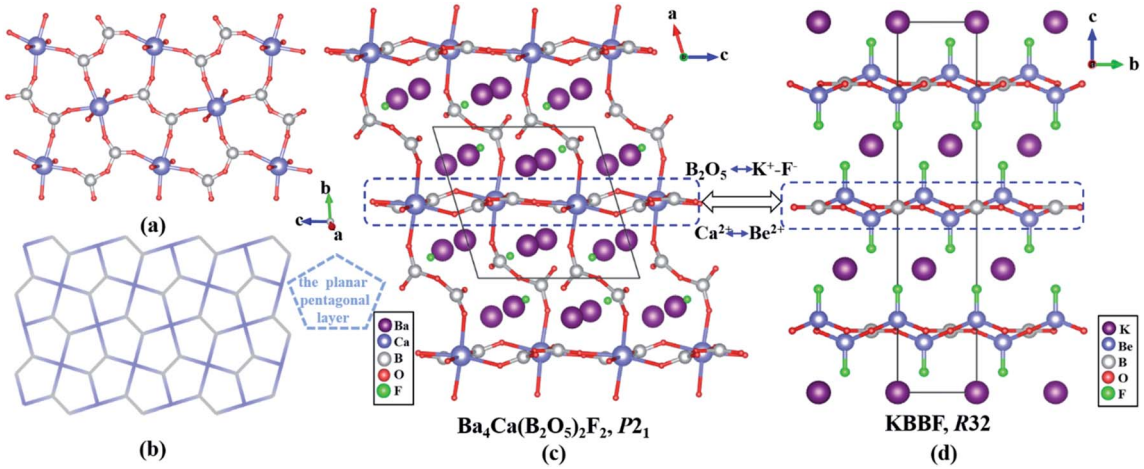

Fig. 1 (a) The $[Ca(B_2O_5)]$ layer is composed of B_2O_5 dimers and CaO_6 octahedra. (b) The planar pentagonal topology layer. The comparison of structures between (c) $Ba_4Ca(B_2O_5)_2F_2$ and (d) KBBF.

$Ba_4Ca(B_2O_5)_2F_2$ is also shown in Fig. 1c and d. In KBBF, the BBUs are the planar BO_3 triangles, which are connected with BeO_3F in the *a*–*b* plane by strong covalent bonds to form the $[Be_2BO_3F_2]_\infty$ layers (Fig. S6c†) and the $[Be_2BO_3F_2]_\infty$ layers have achieved excellent NLO properties of the KBBF crystal.[7] However in $Ba_4Ca(B_2O_5)_2F_2$, the BO_3 triangles are changed into the B_2O_5 dimers, and the BeO_3F tetrahedra are substituted by the CaO_6 polyhedra. These B_2O_5 dimers are also connected by the CaO_6 polyhedra to form the interesting planar pentagonal $[Ca(B_2O_5)]_\infty$ layer (Fig. S6d†). More importantly, in KBBF, the adjacent $[Be_2BO_3F_2]_\infty$ layers are connected by the weak K^+-F^- ionic bonds that results in the strong layer habit of the KBBF crystals, whereas in $Ba_4Ca(B_2O_5)_2F_2$, the $[Ca(B_2O_5)]_\infty$ layers are bridged by the strong covalent B–O bonds to form a stable 3D framework, which will greatly overcome the layering tendency of the KBBF crystal and facilitate the crystal growth.

In addition, we also notice that the planar pentagonal $[Ca(B_2O_5)]_\infty$ layer maybe helpful for enhancing the SHG responses of *pyro*-borates because small SHG responses of *pyro*-borates are attributed to the typical twisted configurations of the B_2O_5 groups, which are unfavorable for forming the π-conjugation and the superposition of the microscopic SHG response. For example, α-$Li_4B_2O_5$, a DUV transparent *pyro*-borate with sole B_2O_5 units as the BBUs, has a weak SHG response, which may be derived from the twisted B_2O_5 groups and non-planar arrangements (Fig. S7a†). However, in $Ba_4Ca(B_2O_5)_2F_2$, the planar configuration of the pentagonal layers can assist the B_2O_5 groups to adopt a nearly coplanar arrangement (Fig. S7b†) and effectively enhance the π-conjugation of B_2O_5 groups. The better π-conjugation of the planar B_2O_5 groups in the planar pentagonal $[Ca(B_2O_5)]_\infty$ layer has also been confirmed by the electron orbital calculation based on the first-principles calculations.[27] The calculated result is shown in Fig. 2. Clearly, the prominent conjugated interactions are observed in the nearly coplanar $B(1,3)_2O_5$ dimers of $Ba_4Ca(B_2O_5)_2F_2$ (Fig. 2a), whereas it does little in the twisted $B(2,4)_2O_5$ dimers of $Ba_4Ca(B_2O_5)_2F_2$ (Fig. 2b) and two types of twisted B_2O_5 dimers in α-$Li_4B_2O_5$ (Fig. 2c and d). It can be expected that the nearly coplanar B_2O_5 dimers are more conducive to the large SHG response than the twisted B_2O_5 dimers. Remarkably, the similar pentagonal layers are also observed in other *pyro*-phosphates, such as $Ba_2NaClP_2O_7$, $K_2Sb(P_2O_7)F$, $Rb_3PbBi(P_2O_7)_2$, and $Rb_3BaBi(P_2O_7)_2$. Clearly, as *pyro*-phosphates are the non-π-conjugated systems, the planar pentagonal layers are only helpful for the orientation of anion groups.[28–31] However, they cannot form the better π-conjugation. Therefore, the better π-conjugation of the nearly coplanar B_2O_5 groups in planar pentagonal layers of *pyro*-borate $Ba_4Ca(B_2O_5)_2F_2$ would have a different contributing mechanism to the SHG effect with other non-π-conjugated *pyro*-phosphates.

The presence of BO_3 triangles in $Ba_4Ca(B_2O_5)_2F_2$ is confirmed by the IR spectral measurements (Fig. S8†). The peaks at 1362 cm^{-1} and 1208 cm^{-1} can be attributed to the asymmetric stretching of BO_3 groups.[32] A strong band at 1069 cm^{-1} in the IR spectrum may be associated with the stretching vibration of B–O–B in B_2O_5.[33,34] The weak absorption bands at 950, and 810 cm^{-1} correspond to the symmetrical stretching vibrations of BO_3 and B–O–B in B_2O_5, respectively. The peaks at 751 and 615 cm^{-1} can be attributed to the out-of-plane bending of the BO_3 groups.[34] Further, the UV-vis-NIR

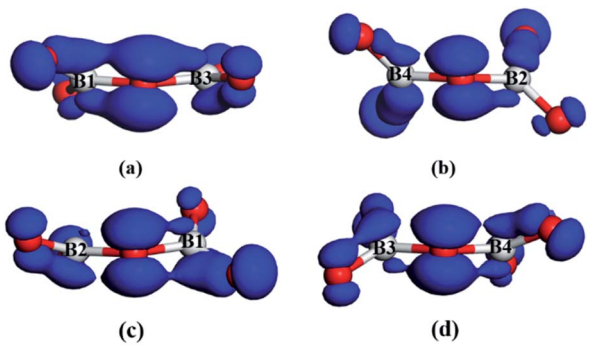

Fig. 2 The orbitals of the nearly coplanar $B(1,3)_2O_5$ (a) and twisted $B(2,4)_2O_5$ dimers (b) in $Ba_4Ca(B_2O_5)_2F_2$. The orbitals of two twisted B_2O_5 dimers (c and d) in α-$Li_4B_2O_5$.

diffuse reflectance spectrum was also measured (Fig. S9†), which shows that $Ba_4Ca(B_2O_5)_2F_2$ is transparent down to the DUV region with a UV cut-off edge less than 190 nm (corresponding to a large band gap of 6.2 eV), which is comparable to the newly developed NLO-active borates, such as $RbB_3O_4F_2$ (<190 nm), $CsZn_2BO_3X_2$ ($X_2 = F_2$,Cl_2, and FCl)) (<190 nm) and so on.[35–38] The short cut-off edge demonstrates the potential application of $Ba_4Ca(B_2O_5)_2F_2$ as a DUV NLO crystal.

As $Ba_4Ca(B_2O_5)_2F_2$ crystalizes in the NCS space group $P2_1$, it possesses the SHG response, which was measured by the Kurtz-Perry method with the well-known NLO material KH_2PO_4 (KDP) as a reference.[39] As shown in Fig. 3, the SHG intensities of $Ba_4Ca(B_2O_5)_2F_2$ increase with the increase of particle sizes, indicating that $Ba_4Ca(B_2O_5)_2F_2$ is type-I phase-matchable. The SHG intensity of $Ba_4Ca(B_2O_5)_2F_2$ at the particle size of 150–212 μm is about 2.2 times that of KDP, and is larger than that of KBBF (1.2 × KDP) or comparable with those newly reported UV NLO crystals, *i.e.* γ-Be_2BO_3F (2.3 × KDP),[6] β-$Rb_2Al_2B_2O_7$ (2 × KDP),[40] $Li_4Sr(BO_3)_2$ (2 × KDP),[41] CsB_4O_6F(~1.9 × KDP).[2] In addition, as we know, the SHG response of $Ba_4Ca(B_2O_5)_2F_2$ is the largest among all the known DUV transparent borates with B_2O_5 units (Table S4†). Its SHG response (2.2 × KDP) is about seven times larger than that of α-$Li_4B_2O_5$ (0.3 × KDP), another DUV transparent *pyro*-borate with sole B_2O_5 units.

To understand the origin of the excellent optical properties of $Ba_4Ca(B_2O_5)_2F_2$, we also carried out the first-principles calculations.[27] It shows that $Ba_4Ca(B_2O_5)_2F_2$ has an indirect band gap of 6.34 eV (Figures S10a†), which is in accordance with the experimental results. The valence band maximum (VBM) of $Ba_4Ca(B_2O_5)_2F_2$ is mainly composed of the orbitals in Ba, and O atoms, while the conduction band minimum (CBM) is dominantly composed of the orbitals in Ba, B, and O atoms. Therefore, the band gap of $Ba_4Ca(B_2O_5)_2F_2$ is mainly determined by Ba atoms and B_2O_5 groups. Based on the calculated electron structure, the NLO coefficients of $Ba_4Ca(B_2O_5)_2F_2$ are also calculated. The largest NLO coefficient of $Ba_4Ca(B_2O_5)_2F_2$ is $d_{22} = -0.524$ pm V^{-1}, which is about 5 times lower than that of α-$Li_4B_2O_5$ ($d_{24} = -0.102$ pm V^{-1}) (Table S5a†), which is matched with the experimental one. Further, the SHG-weighted density maps of $Ba_4Ca(B_2O_5)_2F_2$ are shown in Fig. 4. These reveal that B_2O_5 dimers make the dominant contribution (72.7%) to the total SHG effect (Table S5b†). The band-resolved SHG analysis

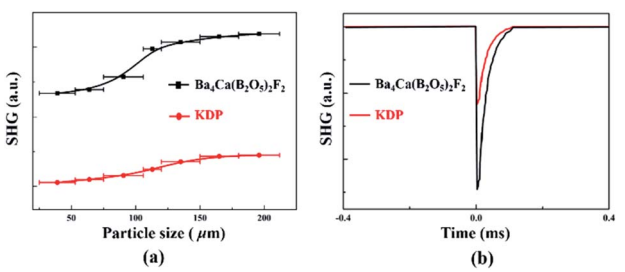

Fig. 3 (a) Phase-matching curve, *i.e.*, particle size *vs.* SHG intensity, data for $Ba_4Ca(B_2O_5)_2F_2$ and KH_2PO_4 (KDP) as reference. The solid curve is a guide for the eye, not a fit to the data. (b) Oscilloscope traces showing SHG intensities for $Ba_4Ca(B_2O_5)_2F_2$ and KDP.

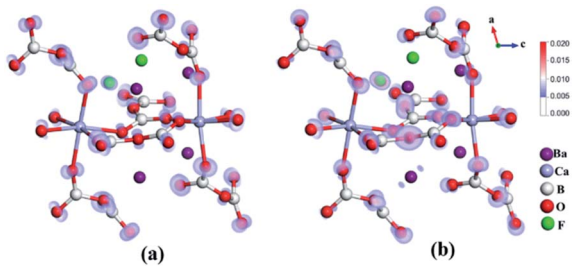

Fig. 4 The SHG-weighted density maps of the virtual electron process (a) and virtual hole process (b) of d_{22} for $Ba_4Ca(B_2O_5)_2F_2$.

can also conclude that B–O orbitals in $Ba_4Ca(B_2O_5)_2F_2$ contribute more to the SHG response than those in α-$Li_4B_2O_5$ (Fig. S10b, S10c†), indicating that the arrangements of B_2O_5 dimers in $Ba_4Ca(B_2O_5)_2F_2$ is more beneficial for the large SHG response. And different from α-$Li_4B_2O_5$, F-centered secondary building units (SBUs) exist in the structure of $Ba_4Ca(B_2O_5)_2F_2$, and they are further linked to construct 2D $[F_2Ba_4]_\infty$ infinite layers, which could help B_2O_5 groups arrange in a planar pattern (Fig. S5†).[26] So, based on the above analysis, we can conclude that the nearly coplanar B_2O_5 dimers in the planar pentagonal layer and the SBU FBa_4 tetrahedra make a significant contribution to the SHG response of $Ba_4Ca(B_2O_5)_2F_2$.

Conclusions

In summary, a new *pyro*-borate $Ba_4Ca(B_2O_5)_2F_2$ with a DUV absorption edge (<190 nm) has been successfully designed and synthesized. Its structure consists of interesting $[Ca(B_2O_5)]_\infty$ layers, which is similar to the $[Be_2BO_3F_2]_\infty$ layers in KBBF. What's more, the $[Ca(B_2O_5)]_\infty$ layers are bridged by the strong covalent B–O bonds to form a stable 3D framework, which would greatly overcome the layering tendency of the KBBF crystal. Based on the electron orbital calculation, better π-conjugated interactions of the B_2O_5 dimers have been confirmed owing to the coplanar requirement of the planar pentagonal layers, which is apparently different from the similar pentagonal layers reported in the *pyro*-phosphates. Further, performance measurements indicate that $Ba_4Ca(B_2O_5)_2F_2$ can exhibit the largest SHG response (2.2 × KDP) in the DUV transparent borates with B_2O_5 units, and its SHG response is about seven times larger than that of α-$Li_4B_2O_5$. The first-principles calculations and the structure–property relationship analysis indicate that the large SHG response of $Ba_4Ca(B_2O_5)_2F_2$ mainly derives from the synergistic effects of the π-conjugated interactions of B_2O_5 dimers in the planar pentagonal layers and the fluorine-centered SBUs. These results suggest that $Ba_4Ca(B_2O_5)_2F_2$ would be a promising UV or DUV NLO crystal. Further research for the large size crystal growth of $Ba_4Ca(B_2O_5)_2F_2$ is also on the way.

Data availability

Supporting data for this article is presented in the ESI.†

Author contributions

Conceptualization and supervision: H. W. Yu and H. P. Wu; synthesis and characterization (single-crystal XRD, powder XRD, TG-DSC, IR, UV-vis-NIR and SHG measurements): S. S. Li; theoretical calculations: X. M. Liu, and Z. S. Lin. All authors proof-read, provided comments, and approved the final version of this manuscript.

Conflicts of interest

The authors declare no conflict of interest.

Acknowledgements

This work was supported by the National Natural Science Foundation of China (Grant Nos. 22071179, 51972230, 51890864, 51802217, 61835014, and 51890865), Natural Science Foundation of Tianjin (Grant Nos. 20JCJQJC00060 and 19JCZDJC38200), and the National Key R&D Program (Grant No. 2016YFB0402103) for this work.

Notes and references

1 H. Wu, H. Yu, Z. Yang, X. Hou, X. Su, S. Pan, K. R. Poeppelmeier and J. M. Rondinelli, *J. Am. Chem. Soc.*, 2013, **135**, 4215–4218.
2 X. Wang, Y. Wang, B. Zhang, F. Zhang, Z. Yang and S. Pan, *Angew. Chem., Int. Ed.*, 2017, **56**, 14119–14123.
3 H. Lu, R. Gautier, M. D. Donakowski, T. T. Tran, B. W. Edwards, J. C. Nino, P. S. Halasyamani, Z. Liu and K. R. Poeppelmeier, *J. Am. Chem. Soc.*, 2013, **135**, 11942–11950.
4 P. S. Halasyamani and K. R. Poeppelmeier, *Chem. Mater.*, 1998, **10**, 2753–2769.
5 B. Zhang, G. Shi, Z. Yang, F. Zhang and S. Pan, *Angew. Chem., Int. Ed.*, 2017, **56**, 3916–3919.
6 G. Peng, N. Ye, Z. Lin, L. Kang, S. Pan, M. Zhang, C. Lin, X. Long, M. Luo, Y. Chen, Y. H. Tang, F. Xu and T. Yan, *Angew. Chem., Int. Ed.*, 2018, **57**, 8968–8972.
7 W. Yao, R. He, X. Wang, Z. Lin and C. Chen, *Adv. Opt. Mater.*, 2014, **2**, 411–417.
8 C. Chen, Y. Wu and R. Li, *J. Cryst. Growth*, 1990, **99**, 790–798.
9 C. Chen, Z. Lin and Z. Wang, *Appl. Phys. B: Lasers Opt.*, 2005, **80**, 1–25.
10 C. Chen, N. Ye, J. Lin, J. Jiang, W. Zeng and B. Wu, *Adv. Mater.*, 1999, **11**, 1071–1078.
11 H. Wu, S. Pan, K. R. Poeppelmeier, H. Li, D. Jia, Z. Chen, X. Fan, Y. Yang, J. M. Rondinelli and H. Luo, *J. Am. Chem. Soc.*, 2011, **133**, 7786–7790.
12 M. Mutailipu, M. Zhang, B. Zhang, L. Wang, Z. Yang, X. Zhou and S. Pan, *Angew. Chem., Int. Ed.*, 2018, **57**, 6095–6099.
13 H. Liu, Y. Wang, B. Zhang, Z. Yang and S. Pan, *Chem. Sci.*, 2020, **11**, 694–698.
14 M. Luo, F. Liang, Y. Song, D. Zhao, F. Xu, N. Ye and Z. Lin, *J. Am. Chem. Soc.*, 2018, **140**, 3884–3887.
15 G. Shi, Y. Wang, F. Zhang, B. Zhang, Z. Yang, X. Hou, S. Pan and K. R. Poeppelmeier, *J. Am. Chem. Soc.*, 2017, **139**, 10645–10648.
16 H. Huang, J. Yao, Z. Lin, X. Wang, R. He, W. Yao, N. Zhai and C. Chen, *Angew. Chem., Int. Ed.*, 2011, **50**, 9141–9144.
17 Y. Wang, B. Zhang, Z. Yang and S. Pan, *Angew. Chem., Int. Ed.*, 2018, **57**, 2150–2154.
18 E. L. Belokoneva, *Crystallogr. Rev.*, 2005, **11**, 151–198.
19 M. Mutailipu, K. R. Poeppelmeier and S. Pan, *Chem. Rev.*, 2021, **121**, 1130–1202.
20 S. Pan, J. P. Smit, B. Watkins, M. R. Marvel, C. L. Stern and K. R. Poeppelmeier, *J. Am. Chem. Soc.*, 2006, **128**, 11631–11634.
21 M. Zhang, D. An, C. Hu, X. Chen, Z. Yang and S. Pan, *J. Am. Chem. Soc.*, 2019, **141**, 3258–3264.
22 X. Chen, B. Zhang, F. Zhang, Y. Wang, M. Zhang, Z. Yang, K. R. Poeppelmeier and S. Pan, *J. Am. Chem. Soc.*, 2018, **140**, 16311–16319.
23 M. He, H. Okudera, A. Simon, J. Köhler, S. Jin and X. Chen, *J. Solid State Chem.*, 2013, **197**, 466–470.
24 W. Miiller, M. Christensen, A. Khan, N. Sharma, R. B. MacQuart, M. Avdeev, G. J. McIntyre, R. O. Piltz and C. D. Ling, *Chem. Mater.*, 2011, **23**, 1315–1322.
25 X. Zhang, D. Li, H. Wu, Z. Yang and S. Pan, *RSC Adv.*, 2016, **6**, 14205–14210.
26 Y. Wang and S. Pan, *Coord. Chem. Rev.*, 2016, **323**, 15–35.
27 L. Kang, F. Liang, X. Jiang, Z. Lin and C. Chen, *Acc. Chem. Res.*, 2020, **53**, 209–217.
28 J. Chen, L. Xiong, L. Chen and L. M. Wu, *J. Am. Chem. Soc.*, 2018, **140**, 14082–14086.
29 Y. Deng, L. Huang, X. Dong, L. Wang, K. M. Ok, H. Zeng, Z. Lin and G. Zou, *Angew. Chem., Int. Ed.*, 2020, **59**, 21151–21156.
30 L. Qi, Z. Chen, X. Shi, X. Zhang, Q. Jing, N. Li, Z. Jiang, B. Zhang and M.-H. Lee, *Chem. Mater.*, 2020, **32**, 8713–8723.
31 X. Lu, Z. Chen, X. Shi, Q. Jing and M. H. Lee, *Angew. Chem., Int. Ed.*, 2020, **59**, 17648–17656.
32 M. Gao, H. Wu, H. Yu, Z. Hu, J. Wang and Y. Wu, *Sci. China: Chem.*, 2021, **64**, 1184–1191.
33 M. Ding, J. J. Xu, H. Wu, H. Yu, Z. Hu, J. Wang and Y. Wu, *Dalton Trans.*, 2020, **49**, 12184–12188.
34 X. Meng, M. Xia and R. Li, *New J. Chem.*, 2019, **43**, 11469–11472.
35 Z. Lu, F. Zhang, A. Tudi, Z. Yang and S. Pan, *Chem. Commun.*, 2020, **56**, 15333–15336.
36 J. Zhou, Y. Liu, H. Wu, H. Yu, Z. Lin, Z. Hu, J. Wang and Y. Wu, *Angew. Chem., Int. Ed.*, 2020, **59**, 19006–19010.
37 M. Mutailipu, Z. Xie, X. Su, M. Zhang, Y. Wang, Z. Yang, M. R. S. A. Janjua and S. Pan, *J. Am. Chem. Soc.*, 2017, **139**, 18397–18405.
38 P. Gong, L. Kang and Z. Lin, *J. Am. Chem. Soc.*, 2020, **142**, 15157–15163.
39 S. K. Kurtz and T. T. Perry, *J. Appl. Phys.*, 1968, **39**, 3798–3813.
40 T. T. Tran, N. Z. Koocher, J. M. Rondinelli and P. S. Halasyamani, *Angew. Chem., Int. Ed.*, 2017, **56**, 2969–2973.
41 S. Zhao, P. Gong, L. Bai, X. Xu, S. Zhang, Z. Sun, Z. Lin, M. Hong, C. Chen and J. Luo, *Nat. Commun.*, 2014, **5**, 1–7.